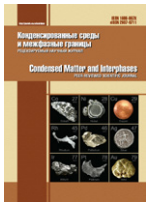

ISSN 1606-867X (Print)
ISSN 2687-0711 (Online)
Condensed Matter and Interphases
Kondensirovannye Sredy i Mezhfaznye Granitsy
https://journals.vsu.ru/kcmf/

Original articles

Research article
https://doi.org/10.17308/kcmf.2026.28/13555

On the formation of the Ag_2Si metastable phase in an Ag-Si film obtained by ion-beam sputtering

K. A. Barkov[1]✉, V. V. Babakov[1], G. P. Potudansky[1], S. A. Ivkov[1], Ya. A. Peshkov[1], I. V. Polshin[1], E. S. Kersnovsky[1], S. Y. Khydyrova[2], K. M. Moiseev[2], I. E. Zanin[1], A. K. Pelagina[1], N. S. Buylov[1], Tran Van Tu[3], A. E. Nikonov[4], A. V. Sitnikov[4]

[1]*Voronezh State University,*
1 Universitetskaya pl., Voronezh 394018, Russian Federation

[2]*Bauman Moscow State Technical University,*
2nd Baumanskaya st., 5, p. 1, Moscow 105005, Russian Federation

[3]*University of Medicine and Pharmacy at Ho Chi Minh city,*
217 Hong Bang Street, Wars 11, District 5, HCMC, Viet Nam

[4]*Voronezh State Technical University,*
84 20 let Oktyabrya st., Voronezh 394006, Russian Federation

Abstract

Objectives: Nanocomposite films based on Ag-Si compounds have application in many areas of science and technology. However, their manufacturing process can be accompanied by the formation of silicides and metastable phases. In this connection, the task of developing methods for their identification arises. In this work, we attempted to solve this task using X-ray diffraction, ultra-soft X-ray emission spectroscopy, and theoretical calculations of the electron density of states for an $Ag_{55}Si_{45}$ film obtained by ion-beam sputtering of a composite target.

Experimental: As a result of comprehensive studies, a nanogranular structure of the film was revealed, with an average silver particle size of ~15 nm, separated by a matrix based on phases of amorphous silicon *a*-Si, SiO_2, and suboxide $SiO_{1.3}$, as well as a silver silicide phase. A comparison of the experimental Si $L_{2,3}$ X-ray emission spectrum of the $Ag_{55}Si_{45}$ film with theoretically calculated spectra of the $AgSi_3$, Ag_2Si, and Ag_3Si phases shows the best agreement with the spectrum of the Ag_2Si phase. Moreover, the Ag_2Si phase was detected in the works of other authors.

Conclusions: Thus, based on X-ray diffraction, X-ray emission spectroscopy, and theoretical calculations of the electronic density of states, it has been established that a metastable Ag_2Si phase is formed in the $Ag_{55}Si_{45}$ film produced by ion-beam sputtering.

Keywords: Metastable Ag-Si-based phases, $AgSi_3$, Ag_2Si, Ag_3Si, silver silicides, ion-beam sputtering, Ultra-soft X-ray emission spectroscopy (USXES), Electronic density of states (DOS)

Funding: This work was funded by the Russian Science Foundation, under grant number 23-79-10294, https://rscf.ru/project/23-79-10294/

Acknowledgments: The research results were partially obtained using the equipment of the Voronezh State University's Center for Collective Use. URL: http://ckp.vsu.ru

For citation: Barkov K. A., Babakov V. V., Potudansky G. P., Ivkov S. A., Peshkov Ya. A., Polshin I. V., Kersnovsky E. S., Khydyrova S. Y., Moiseev K. M., Zanin I. E., Pelagina A. K., Buylov N. S., Tran Van Tu, Nikonov A. E., Sitnikov A. V On the formation of the Ag_2Si metastable phase in an Ag-Si film obtained by ion-beam sputtering. *Condensed Matter and Interphases*. 2026;(1): 15–27. https://doi.org/10.17308/kcmf.2026.28/13555

✉ Konstantin A. Barkov, e-mail: barkov@phys.vsu.ru

Для цитирования: Барков К. А., Бабаков В. В., Потуданский Г. П., Ивков С. А., Пешков Я. А., Польшин И. В., Керсновский Е. С., Хыдырова С. Ю., Моисеев К. М., Занин И. Е., Пелагина А. К., Буйлов Н. С., Tran Van Tu, Никонов А. Е., Ситников А. В. О формировании метастабильной фазы Ag_2Si в пленке Ag-Si, полученной ионно-лучевым распылением. *Конденсированные среды и межфазные границы*. 2026;(1): 15–27. https://doi.org/10.17308/kcmf.2026.28/13555

Introduction

Ag-Si nanocomposite films are currently used in the fabrication of SERS substrates (Surface-enhanced Raman spectroscopy) [1–6], plasmonic reflectors [7, 8], anodes for lithium-ion batteries [9, 10], memristor structures [11–21], as well as electrical synapses for neuromorphic systems [22–24]. At the same time, the phase diagram of the Ag-Si system is of the eutectic type, which should lead to the formation of silver and silicon particles [25]. However, during the formation of nanostructured *Me*-Si films by methods characterized by the high energy of sputtered particles, the formation of metastable compounds [26, 27] and solid solutions, such as Ag_2Si [28–30], is possible. Furthermore, databases also contain information about theoretically calculated phases of silver silicide $AgSi_3$ and Ag_3Si [31, 32], as well as data on the formation of compounds with an unknown crystal structure in works [33, 34]. Based on this, it becomes necessary to investigate the possibility of forming metastable phases of silver silicides in Ag-Si films. Therefore, this work employs the method of ultra-soft X-ray emission spectroscopy to identify the phases of silver silicide in an $Ag_{55}Si_{45}$ film obtained by ion-beam sputtering.

2. Methods

2.1. Method of obtaining Ag-Si film by ion-beam sputtering

An $Ag_{55}Si_{45}$ film with a thickness of about 1 μm was deposited on a Si (100) substrate of KDB-12 grade by ion-beam sputtering of a composite target made of pure Ag (99.99 %) and silicon pieces of Si (KDB-12). To form a film with the required atomic composition – $Ag_{55}Si_{45}$, silicon pieces 10 mm wide were placed on the surface of a silver plate with an 18 mm gap. Deposition was carried out in a vacuum chamber (residual pressure 10^{-6} Torr). The methodology for obtaining Ag-Si films by ion-beam sputtering is described in more detail in our previous work [35].

2.2. Research methods for structure and phase composition

The elemental composition of the film was determined by energy-dispersive spectroscopy (EDS) on a JEOL JSM-6380LV scanning electron microscope (SEM) equipped with an INCA Energy 250 microanalysis system at a primary electron energy of 5 keV. This energy value was chosen to perform elemental analysis exclusively within the film volume. SEM imaging was performed at an accelerating voltage of 20 kV.

An analysis of the formation of crystalline phases in the $Ag_{55}Si_{45}$ sample was carried out by X-ray diffraction on a PANalytical Empyrean B.V. diffractometer with Cu$K\alpha_{1,2}$ radiation $\lambda = 1.542$ Å.

The phase composition of the $Ag_{55}Si_{45}$ film was determined using a unique technique of ultra-soft X-ray emission spectroscopy (USXES), implemented on an RSM-500 spectrometer. The USXES method provides information on the distribution of Si 3*s* states in the valence band based on the Si $L_{2,3}$ X-ray emission spectrum [36, 37]. As a result of the simulation of the experimental spectra, the USXES method allows for the identification of the presence of crystalline and amorphous silicon phases, as well as silicides and silicon oxides in the surface layers from 10 to 120 nm [38].

2.3. The method for calculating the electron density of states in the valence band

The calculations of the electron density of states and the Si $L_{2,3}$ X-ray emission spectra for the $AgSi_3$, Ag_2Si, and Ag_3Si phases were carried out within the framework of density functional theory using the linearized augmented plane wave (LAPW) method. In this work, the calculations were performed using the PBE-GGA generalized gradient approximation for the exchange-correlation energy in the Wien2k software package [39]. The crystal potential was constructed as a full potential, accounting for anisotropy, which allows the LAPW method to calculate compounds with directional covalent bonds, such as silicon-based compounds.

3. Results and discussion

3.1. Analysis of the elemental and phase composition of the Ag-Si film

Analysis of the elemental composition of the $Ag_{55}Si_{45}$ film by energy-dispersive spectroscopy confirms the Ag:Si = 55:45 ratio. As a result of ion-beam sputtering of a composite target based on Ag and Si under the specified conditions, the formed surface of the $Ag_{55}Si_{45}$ film has a continuous and homogeneous structure with uniform graininess and a characteristic grain size of 50–200 nm, as seen on the SEM image of the surface in Fig. 1a. The film thickness is ~0.8 μm (Fig. 1b). The nanogranular structure of the pure silver film is explained by the specifics of the ion-beam sputtering technology, during which nanoclusters of the target material several nanometers in size are predominantly sputtered from the target; these nanoclusters possess sufficiently high energy upon reaching the substrate and can form metastable phases. Therefore, X-ray structural and X-ray spectral studies were conducted to analyze the presence of metastable compounds in the formed $Ag_{55}Si_{45}$ film.

Fig. 2a shows the X-ray diffraction patterns of the ion-beam $Ag_{55}Si_{45}$ film, pure Ag, polycrystalline silicon (poly-Si), and the silver silicide phases $AgSi_3$, Ag_2Si, and Ag_3Si. The diffraction patterns of the $AgSi_3$, Ag_2Si, and Ag_3Si phases were theoretically calculated using the Vesta program [40], based on the unit cells published in the Springer Materials [41] and Materials Explorer [31, 32] databases. The X-ray diffraction pattern of the $Ag_{55}Si_{45}$ film shows diffraction peaks at 2θ = 37.98° and 64.35°, corresponding to the interplanar spacings d = 2.367 and 1.448 Å. These reflections are associated with the Ag (111) and Ag (220) crystallographic planes, respectively [ICDD (International Centre for Diffraction Data), PDF-2 Database, Card No. 00-004-0783]. The Ag diffraction peaks in the $Ag_{55}Si_{45}$ film are significantly broadened (FWHM Ag (111) = 0.66 2θ deg.) compared to the corresponding peaks in the pure silver reference (FWHM Ag (111) = 0.12 2θ deg.), indicating a small silver crystallite size, which, according to the Debye-Scherrer method [42], is ~15 nm. However, in the angular region of 39–40°, the Ag (111) reflection has a shoulder. Moreover, the decomposition of the Ag (111) reflection into the Cu$K\alpha_1$,α_2 doublet lines by Lorentz functions indeed reveals an additional reflection with an interplanar spacing of 2.314 Å (top inset in Fig. 2). The most intense reflections from the $AgSi_3$, Ag_2Si, and Ag_3Si phase diffractograms are located in this angular region (Fig. 2). Furthermore, the Ag (200) reflection in the $Ag_{55}Si_{45}$ film is broadened more strongly compared to the Ag (111) and Ag (220) reflections, which is clearly seen from the $\beta \times \cos\theta$ vs. $\sin\theta$ dependence (bottom inset in Fig. 2) constructed using the Williamson-Hall method [43]. (The diffractogram of the $Ag_{55}Si_{45}$ sample, recorded over a larger angular range, is shown in Fig. S1 in the supplementary materials file). The large half-width of the Ag (200) reflection in the $Ag_{55}Si_{45}$ film may be due to the contribution of reflections from the $AgSi_3$

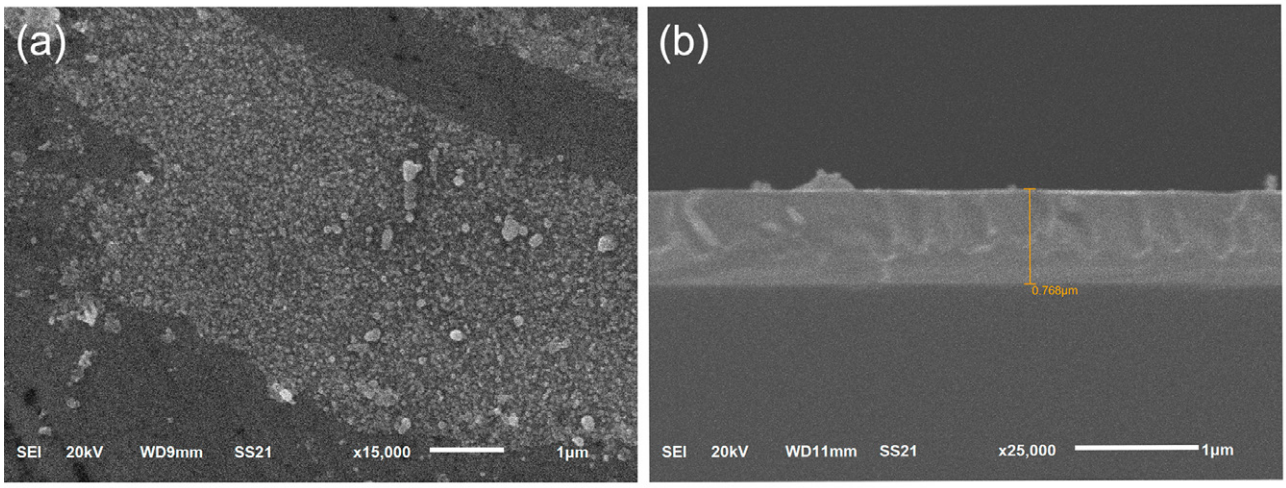

Fig. 1. SEM micrographs of the surface (a) and fracture (b) of the $Ag_{55}Si_{45}$ ion-beam deposited film

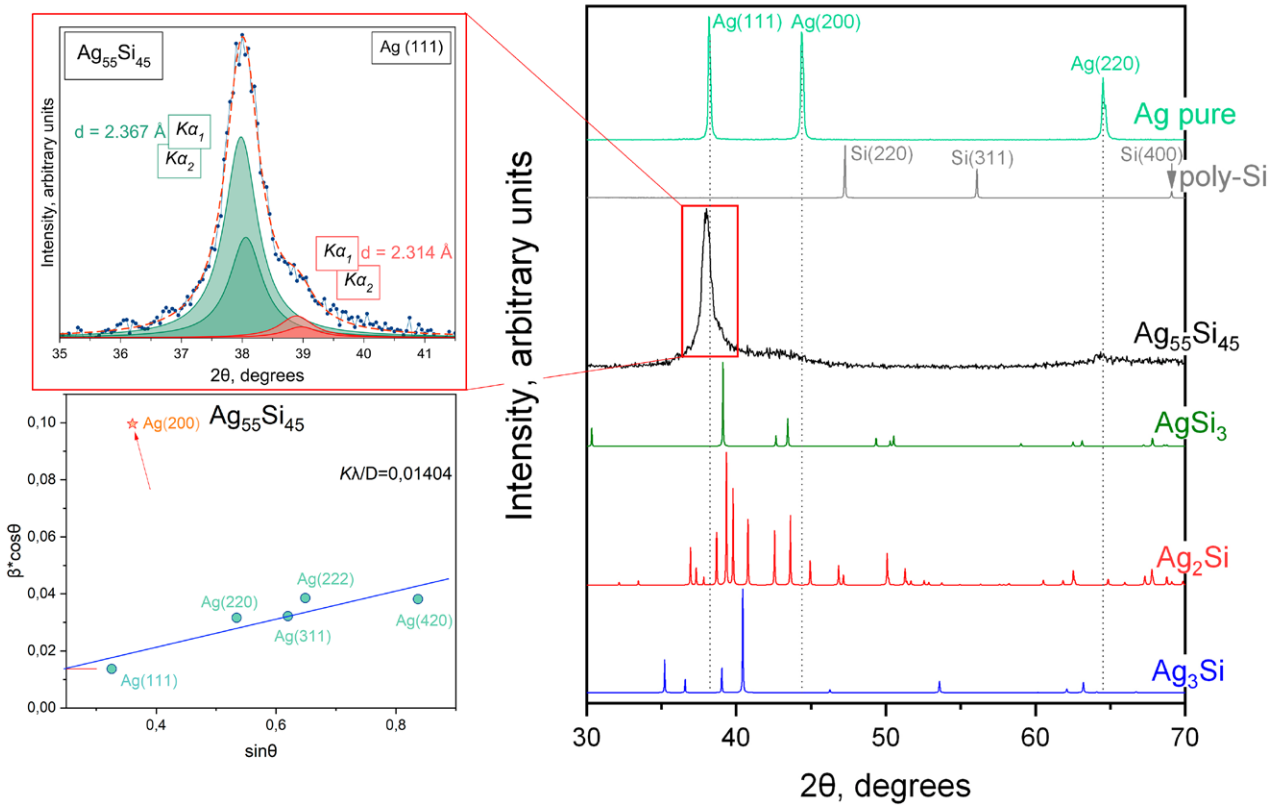

Fig. 2. X-ray diffractograms of the $Ag_{55}Si_{45}$ film, reference standards of pure silver (Ag) and polycrystalline silicon (poly-Si), as well as silver silicides $AgSi_3$, Ag_2Si, and Ag_3Si [31, 41, 32]. The top inset shows the X-ray diffractogram in the region of the Ag (111) reflection. The bottom inset presents the calculation of crystallite size and lattice microstrain using the Williamson–Hall method

and Ag_2Si phases located in the angular region of 43–44°. Moreover, for the $Ag_{55}Si_{45}$ sample, the Williamson-Hall method, based on the universal deformation model (UDM) [43], reveals the presence of a microstrain of the crystal lattice of ~ 1.2 %, while the size of the Ag nanocrystals is ~ 11 nm, which is in good agreement with the Debye–Scherrer method.

The combination of such factors as the overestimated value of the full width at half maximum for the Ag (200) reflex, as well as the asymmetry of the Ag (111) diffraction reflex, with the detection of an additional reflex with an interplanar spacing value of 2.314 Å, may indicate the formation of $AgSi_3$, Ag_2Si, and Ag_3Si phases in the $Ag_{55}Si_{45}$ film, whose most intense reflexes are located in the region of the considered Ag (111) and Ag (200) reflexes (Fig. 2). However, according to X-ray diffraction data, it is almost impossible to attribute the noted features to any specific silver silicide phase ($AgSi_3$, Ag_2Si, or Ag_3Si). Therefore, for the unambiguous identification of the silver silicide phase formed in the $Ag_{55}Si_{45}$ film, X-ray emission Si $L_{2,3}$-spectra will be obtained. However, due to the lack of published X-ray emission Si $L_{2,3}$-spectra for the $AgSi_3$, Ag_2Si, and Ag_3Si phases, theoretical calculations of the electronic density of states and X-ray spectra will be performed.

3.2. Calculation of the electron density of states in the valence band of metastable compounds $AgSi_3$, Ag_2Si, and Ag_3Si

To calculate the electronic density of states (DOS) for the $AgSi_3$ phase, a tetragonal unit cell (Fig. 3a) with the space group symmetry (*I4/mmm*, 139) and lattice parameters $a = b = 4.16$ Å, $c = 7.38$ Å, $\alpha = \beta = \gamma = 90°$ was used. The structural data and atomic coordinates (Table TS1) for the $AgSi_3$ phase (*I4/mmm*, 139) were taken from the Materials Explorer database [31]. In $AgSi_3$, silver atoms are located at the vertices of the tetragonal unit cell, and silicon atoms occupy

two nonequivalent positions, $Si^{(1)}$ and $Si^{(2)}$, with different distances to the nearest silver atom of 2.78 and 2.94 Å, respectively. The DOS of the $AgSi_3$ phase is mainly determined by the density of silver *d*-states, which are highly localized and have a maximum at ~ 5.5 eV below E_F, as well as by the silicon *s*- and *p*-states (Fig. 3b). The DOS of the silicon atoms $Si^{(1)}$ and $Si^{(2)}$ in $AgSi_3$ is almost identical (Fig. 3c, e), with the highest density of *s*-states concentrated in the region of 6–13 eV below E_F, and *p*-states in the region of 0–6 eV below E_F with a maximum at -6 eV. Such a DOS is characteristic of higher transition metal silicides [44-46]. The difference in the partial DOS of the *s*- and *p*-states of the $Si^{(1)}$ and $Si^{(2)}$ atoms (Fig. 3d) is due to the difference in the local atomic environment. Fig. 3f shows the X-ray emission spectrum of the $AgSi_3$ phase calculated by us, which was compared with the obtained experimental spectrum of the $Ag_{55}Si_{45}$ film.

The orthorhombic unit cell (Fig. 4a) with the space group (*Cmcm*, 63) and lattice parameters $a = 5.56$ Å, $b = 9.16$ Å, $c = 8.49$ Å, $\alpha = \beta = \gamma = 90°$ was used for the calculation of the DOS for the Ag_2Si

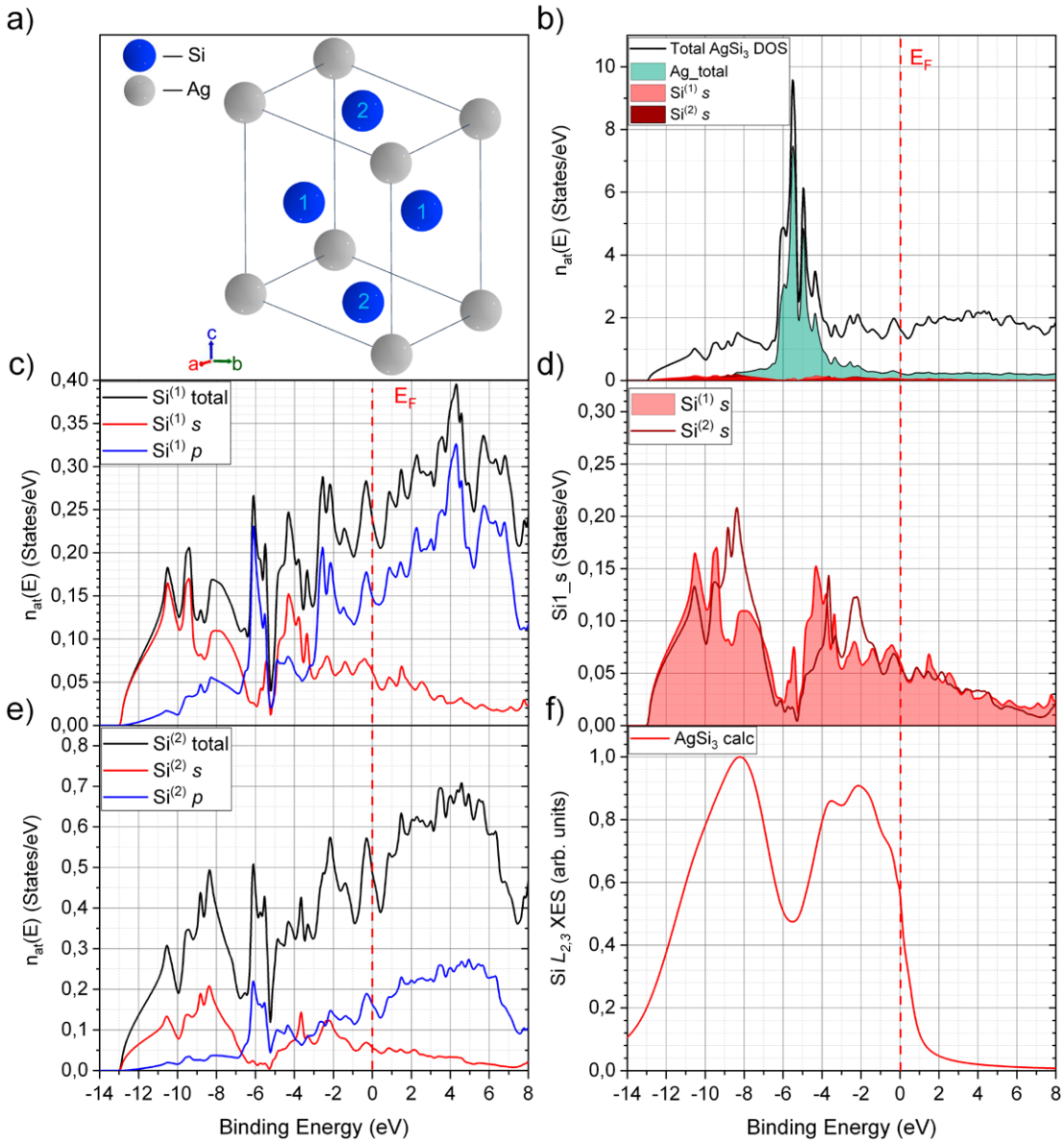

Fig. 3. Unit cell (a), partial and total densities of states for $Si^{(n)}$ atoms (c, d, e). Total DOS for Ag and $AgSi_3$, as well as s-states for $Si^{(n)}$ atoms (b). Calculated X-ray emission Si $L_{2,3}$-spectrum of the $AgSi_3$ phase (*I4/mmm*, 139) (f)

phase. The structural data and atomic coordinates (Table TS2) for the Ag_2Si phase (*Cmcm*, 63) were taken from the Springer Materials database [41]. In this unit cell, Ag atoms occupy three non-equivalent positions: $Ag^{(1)}$ and $Ag^{(3)}$ atoms are located the farthest from the silicon atoms (3.09 and 3.06 Å, respectively); $Ag^{(2)}$ atoms are located the closest to the Si atoms at a distance of 3.01 Å. The total and partial DOS were calculated for each $Ag^{(n)}$ atom in the Ag_2Si compound (Fig. 4b, d, f). The DOS of each $Ag^{(n)}$ atom is mainly formed by *d*-states and contains four maxima: *A* (*E* ~ -2.8 eV), *B* (*E* ~ -3.5 eV), *C* (*E* ~ - 4.5 eV) and *D* (*E* ~ -5.7 eV). At the same time, for all $Ag^{(n)}$ atoms, a deviation in the intensity ratio and a shift of ~ 1 eV towards low *E* values of the DOS maxima are observed compared to bulk FCC Ag (Fig. S2). These changes in the DOS of the $Ag^{(n)}$ atoms result from hybridization with each other (for example, in the case of $Ag^{(3)}$ atoms, mainly with $Ag^{(2)}$ atoms), as well as with silicon atoms, as can be seen from the DOS of the $Ag^{(2)}$ atoms, where peak *B* becomes the main one due to the hybridization of Ag *d* and Si *s*-states (Fig. 4d). The result of this hybridization is noticeably reflected in the partial DOS of Si *s*-states, where an intense peak appears

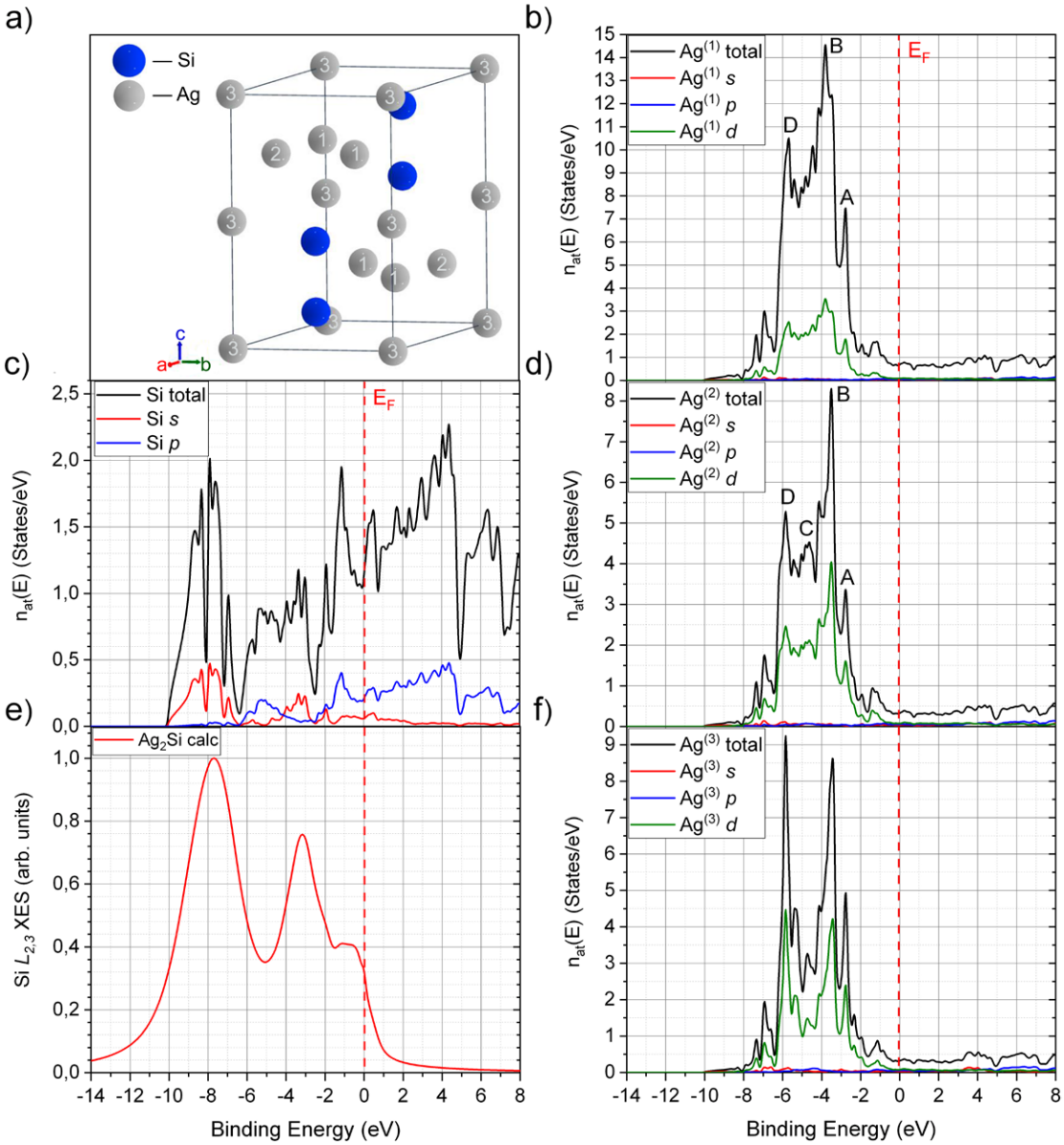

Fig. 4. Unit cell (a), partial and total DOS for $Ag^{(n)}$ atoms (b, d, f), Si atoms (c), and the calculated X-ray emission Si $L_{2,3}$-spectrum of the Ag_2Si phase (*Cmcm*, 63) (e)

at -3 eV (Fig. 4c). The presence of this peak is also observed in the calculated X-ray Si $L_{2,3}$ emission spectrum of the Ag_2Si phase (Fig. 4f).

For the calculation of the DOS for the Ag_3Si phase, a hexagonal unit cell (Fig. 5a) with the space group symmetry (*P*-6*m*2, 187) and lattice parameters $a = b = 2.94$ Å, $c = 9.22$ Å, $\alpha = \beta = 90°$, $\gamma = 120°$ was used. The structural data and atomic coordinates (Table TS3) for the Ag_3Si phase (*P*-6*m*2, 187) were taken from the Materials Explorer database [32]. In the unit cell of the Ag_3Si phase, silver atoms occupy two non-equivalent positions, $Ag^{(1)}$ and $Ag^{(2)}$ (Fig. 5a). The DOS of both $Ag^{(1)}$ and $Ag^{(2)}$ atoms is localized in the region of 2–8 eV below E_F (Fig. 5c, e) and defines the total density of states of the Ag_3Si phase. However, due to the close proximity of $Ag^{(1)}$ atoms to silicon atoms (2.77 Å), their partial DOS differs most significantly from that of bulk silver with an FCC structure (Fig. 5c and Fig. S2) and has a main maximum at -3 eV. At the same time, the $Ag^{(2)}$ atoms in the Ag_3Si phase are located in the same layer and are surrounded by silver atoms, which results in a DOS character close to that of

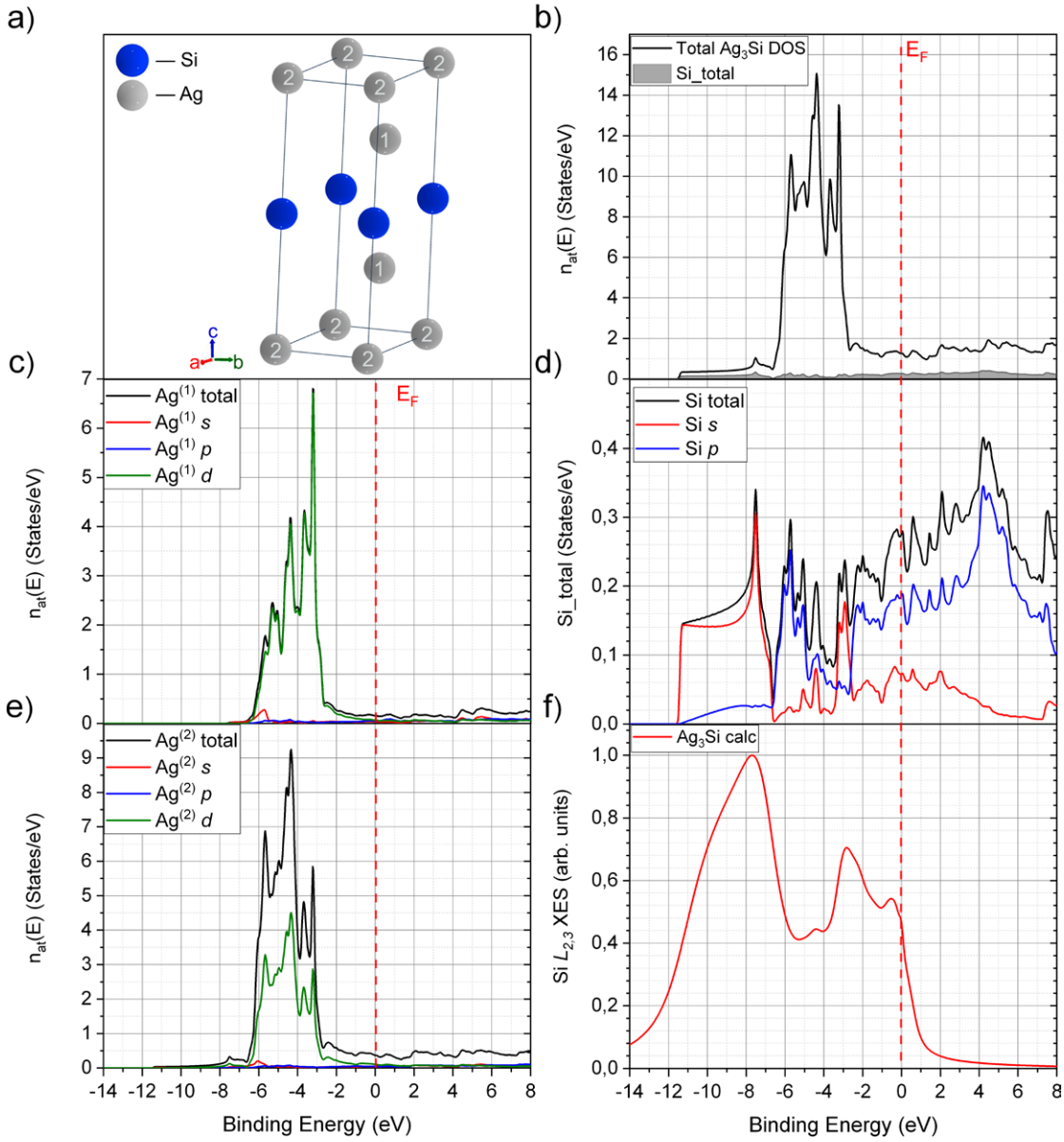

Fig. 5. Unit cell (a), partial and total DOS for $Ag^{(n)}$ atoms (c, e) and Si atoms (d). Total density of states for Ag_3Si and Si (b), calculated X-ray emission Si $L_{2,3}$-spectrum of the Ag_3Si phase (*P*-6*m*2, 187) (f)

bulk Ag (Fig. 5e). The Si *3p* DOS is concentrated in the region from 0 to –8 eV and has a maximum at -6 eV (Fig. 5d). The density of *s*-states of Si atoms in Ag_3Si is mostly concentrated in the range of 6–12 eV below E_F with a maximum at ~ -7.5 eV (Fig. 5d). Furthermore, the *s*-states have an additional maximum at ~ –3–3.5 eV, caused by hybridization with *d*-states, which is clearly manifested in the calculated X-ray Si $L_{2,3}$ emission spectrum (Fig. 5f).

Thus, using the linearized augmented plane wave method, the Si $L_{2,3}$ X-ray emission spectra for the $AgSi_3$, Ag_2Si and Ag_3Si phases were theoretically calculated, reflecting the partial density of electronic *s*-states. The spectra of all silver silicides have two distinct intensity maxima at ~ 7–8 eV (the main maximum) and at ~ 2–3 eV below E_F. The presence of the low-energy maximum is due to the result of hybridization of Si *s* and Ag *d*-states. To compare the calculated Si $L_{2,3}$ X-ray emission spectra with the experimental ones obtained by the USXES method, their energy scales were aligned taking into account the Si *2p* level binding energy of 99.9 eV [47].

3.3. Identification of silver silicides in Ag-Si film by USXES

Fig. 6a presents the ultrasoft X-ray emission Si $L_{2,3}$-spectra of the $Ag_{55}Si_{45}$ film obtained at an analysis depth of 60 nm (black dots). To identify the formation of the silver silicide phase in the $Ag_{55}Si_{45}$ film, computer simulation of the X-ray emission Si $L_{2,3}$-spectrum was performed based on reference spectra. The theoretically calculated spectra of silver silicides $AgSi_3$, Ag_2Si, and Ag_3Si, as well as the spectra of amorphous silicon *a*-Si, dioxide SiO_2, and suboxide $SiO_{1.3}$ of silicon (Fig. 6b) were used as reference spectra, the presence of which in Ag-Si films is possible according to previous studies [35]. The simulation of the X-ray emission Si $L_{2,3}$-spectrum of the $Ag_{55}Si_{45}$ film was performed three times, using only one spectrum of silver silicide $AgSi_3$, Ag_2Si, or Ag_3Si, as well as the spectra of the *a*-Si, SiO_2 and $SiO_{1.3}$ phases in the ratio that best describes the experimental spectrum according to the method [38]. Simulated spectra obtained using the $AgSi_3$, Ag_2Si, and Ag_3Si standards are presented in Fig. 6a as green, red, and blue lines, respectively, and the simulation

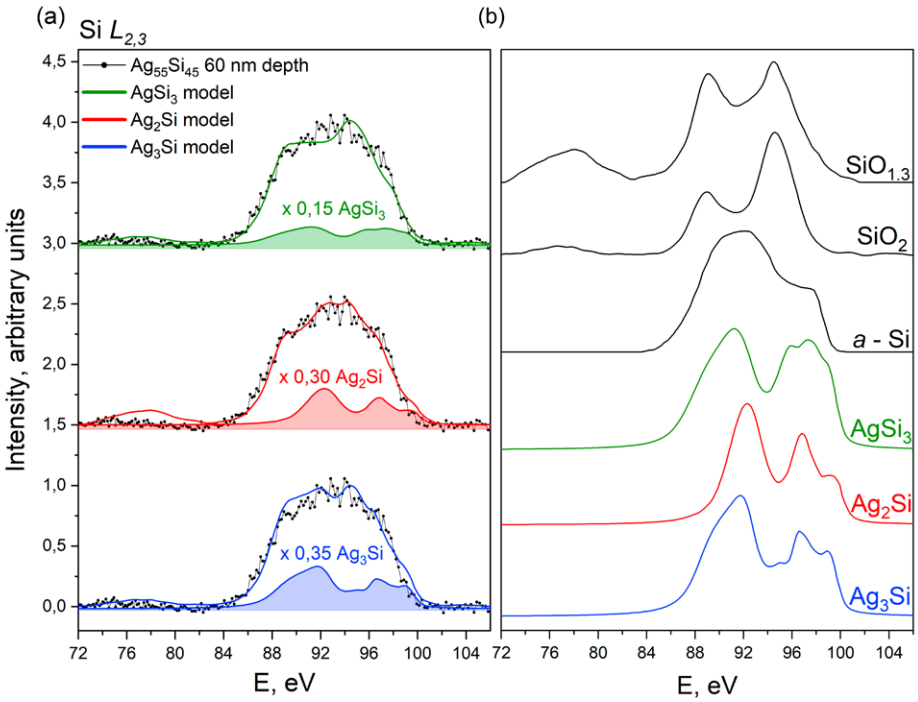

Fig. 6. X-ray emission Si $L_{2,3}$-spectra of the $Ag_{55}Si_{45}$ film obtained at an analysis depth of 60 nm, as well as spectra obtained through computer modeling (a). Spectra of reference standards: silicon suboxide ($SiO_{1.3}$), silicon dioxide (SiO_2), amorphous silicon (*a*-Si), and theoretically calculated spectra of silver silicides ($AgSi_3$, Ag_2Si, and Ag_3Si). The experimental spectrum is represented by dots, the model – by solid lines of various colors (b)

results are given in Table 1. It can be seen from Fig. 6a that the simulation using the $AgSi_3$ spectrum (green curve) fails to describe the experimental spectrum of the $Ag_{55}Si_{45}$ film in the region of the main maximum (89–93 eV), as well as near the top of the valence band (96–98 eV). At the same time, this simulation variant reveals about 15 % of the $AgSi_3$ phase in the $Ag_{55}Si_{45}$ film (Table 1). At the same time, the simulated spectrum using the Ag_2Si standard allows to describe all the features of the experimental spectrum (Fig. 6a, red curve) and reveals about 30 % of the Ag_2Si phase in the $Ag_{55}Si_{45}$ film (Table 1). Using the reference spectrum of the Ag_3Si phase for simulation also reveals a fairly high content of this silver silicide (35 %); however, the simulated spectrum has a higher intensity in the region of 89–92 eV relative to the experimental one, which does not allow this model to be considered reliable (Fig. 6a, blue curve). Thus, based on the modeling results of the Si $L_{2,3}$ X-ray emission spectrum of the $Ag_{55}Si_{45}$ film, it was found that the best agreement between the simulated spectrum and the experiment is achieved when using the reference spectrum of Ag_2Si. However, due to the presence of statistical intensity fluctuations characteristic of a limited signal acquisition time, as well as the inclusion of multiple components in the model, for clarity, a comparison of the spectral feature positions of the reference spectra $AgSi_3$, Ag_2Si, and Ag_3Si with the difference spectra of the $Ag_{55}Si_{45}$ film (Fig. 7) was performed. The difference spectra of the $Ag_{55}Si_{45}$ film (Fig. 7, black dots) were obtained by subtracting the SiO_2, $SiO_{1.3}$, and *a*-Si components from the experimental spectrum in the proportion indicated in Table 1. It can be

Table 1. Phase composition of the $Ag_{55}Si_{45}$ film based on the modeling of the X-ray emission Si $L_{2,3}$-spectrum using three different silver silicide references: $AgSi_3$, Ag_2Si, and Ag_3Si

The silver silicide spectrum used in the model	Phase composition					
	SiO_2, %	$SiO_{1.3}$, %	*a*-Si, %	$AgSi_3$, %	Ag_2Si, %	Ag_3Si, %
$AgSi_3$	45	5	35	15	–	–
Ag_2Si	20	30	20	–	30	–
Ag_3Si	40	5	20	–	–	35

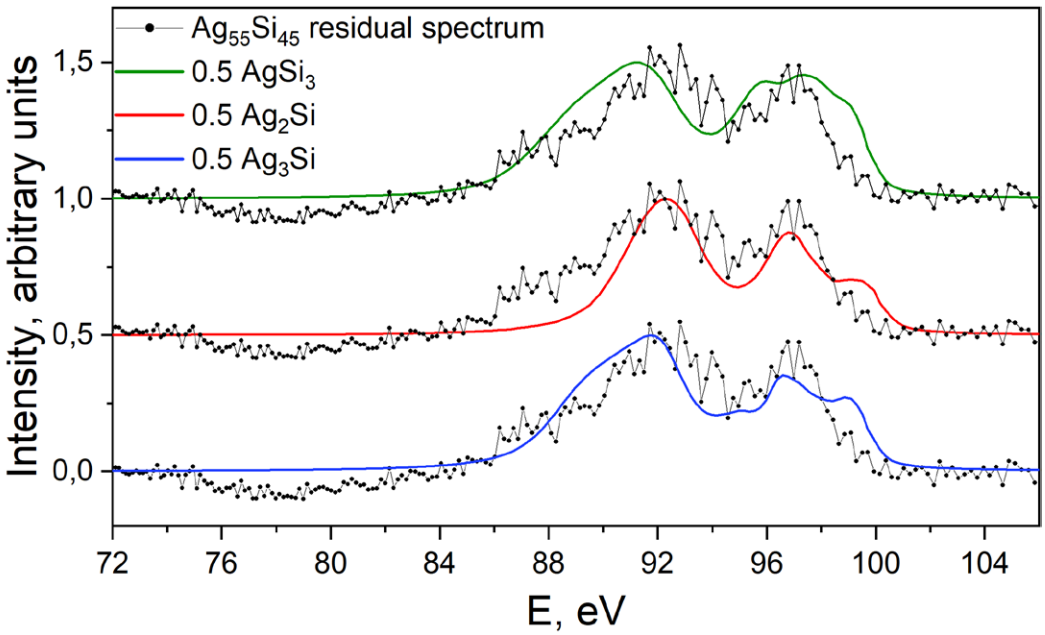

Fig. 7. Residual spectra of the $Ag_{55}Si_{45}$ film after subtraction of the *a*-Si, $SiO_{1.3}$, and SiO_2 components, as well as the spectra of silver silicides $AgSi_3$ (green line), Ag_2Si (red line), and Ag_3Si (blue line). The experimental spectrum is represented by dots

seen from Fig. 7 that the difference spectra of the $Ag_{55}Si_{45}$ film have two intensity maxima at ~ 92 and 97 eV. The spectra of all silicides also reveal the presence of two intensity maxima in the given energy regions. However, the high-energy maximum of the $AgSi_3$ phase is strongly broadened compared to the difference spectrum and has a high density of states near the top of the valence band, which is characteristic of higher silicides [48]. In turn, the spectrum of the Ag_2Si phase demonstrates similarity in the position and width of the intensity maxima to the difference spectrum (Fig. 7). The spectrum of the Ag_3Si phase also shows agreement in the position with the main and additional maxima of the difference spectrum of the $Ag_{55}Si_{45}$ film, and the main difference lies in the high intensity near the top of the VB. Differences in the intensity of the Si $L_{2,3}$ spectra near VB indicate the absence of the Ag_3Si phase in the studied sample.

Thus, due to the best agreement between the experimental Si $L_{2,3}$ X-ray emission spectrum of the $Ag_{55}Si_{45}$ film and the reference spectrum of the Ag_2Si phase, the formation of this metastable phase in the Ag-Si film during ion-beam sputtering of a composite target has been established. It should be noted, however, that the possibility of forming other silicides in Ag-Si films cannot be completely ruled out, although their detection is a challenging task.

4. Conclusions

As a result of X-ray diffraction studies of the $Ag_{55}Si_{45}$ film, obtained by ion-beam sputtering of a composite Ag-Si target, it was found that the film consists of silver nanoparticles with an average size of ~ 15 nm, as well as a solid solution based on Ag-Si, as evidenced by an additional reflex on the diffractogram in the angular range where the main maxima of the $AgSi_3$, Ag_2Si, and Ag_3Si phases are located. However, according to X-ray diffraction data, it is almost impossible to unambiguously identify the phase of silver silicide formed in the film.

At the same time, the analysis of X-ray emission Si $L_{2,3}$-spectra shows that the $Ag_{55}Si_{45}$ film is a complex composite material and contains phases of amorphous silicon *a*-Si, SiO_2, suboxide $SiO_{1.3}$, as well as a significant presence (~ 30 % of the total number of silicon atoms) of the silver silicide phase. Comparison of the experimental X-ray emission Si $L_{2,3}$-spectrum of the $Ag_{55}Si_{45}$ film with the theoretically calculated spectra of the $AgSi_3$, Ag_2Si, and Ag_3Si phases shows the best agreement with the spectrum of the Ag_2Si phase. Moreover, the Ag_2Si phase was identified by the authors of studies [26, 28–30].

Thus, based on X-ray diffraction data, X-ray emission spectroscopy, and theoretical calculations of the electronic density of states, it has been established that a metastable Ag_2Si phase is formed in the $Ag_{55}Si_{45}$ film produced by ion-beam sputtering.

Contribution of the authors

The authors contributed equally to this article.

Conflict of interests

The authors declare that they have no known competing financial interests or personal relationships that could have influenced the work reported in this paper.

The online version https://journals.vsu.ru/kcmf *contains supplementary material*

References

1. Yang Z. W., Meng L. Y., Lin J. S., ... Li J. F. 3D hotspots platform for plasmon enhanced Raman and second harmonic generation spectroscopies and quantitative analysis. *Advanced Optical Materials*. 2019;7: 3–8. https://doi.org/10.1002/adom.201901010

2. Ermina A. A., Solodovchenko N. S., Levitskii V. S., ... Zharova Y. A. Plasmonic disordered array of hemispherical AgNPs on SiO_2@c-Si: their optical and SERS properties. *Materials Science in Semiconductor Processing*. 2024;169: 107861. https://doi.org/10.1016/j.mssp.2023.107861

3. Dzhagan V., Mazur N., Kapush O., ... Yukhymchuk V. Self-organized SERS substrates with efficient analyte enrichment in the hot sSpots. *ACS Omega*. 2024;9(4): 4819–4830. https://doi.org/10.1021/acsomega.3c08393

4. Kukushkin V. I., Van'kov A. B., Kukushkin I. V. Relationship between the giant enhancement of the Raman scattering and luminescence on nanostructured metallic surfaces. *Journal of Experimental and Theoretical Physics Letters*. 2013;98(6): 342–347. https://doi.org/10.1134/S0021364013190089

5. Ghosh R., Ghosh J., Das R., ... Giri P. K. Multifunctional Ag nanoparticle decorated Si nanowires for sensing, photocatalysis and light emission applications. *Journal of Colloid and Interface Science*. 2018;532: 464-473. https://doi.org/10.1016/j.jcis.2018.07.123

6. Poletaeva D. A., Khakina E. A., Kukushkin V. I., ... Kotelnikov A. I. Application of SERS spectroscopy for detection of water-soluble fullerene C60 derivatives and

their covalent conjugates with dyes. *Doklady Physical Chemistry*. 2015;460(1): 1–5. https://doi.org/10.1134/S0012501615010017

7. Morawiec S., Mendes M. J., Priolo F., Crupi I. Plasmonic nanostructures for light trapping in thin-film solar cells. *Materials Science in Semiconductor Processing*. 2019;92: 10–18. https://doi.org/10.1016/j.mssp.2018.04.035

8. Atwater H. A., Polman A. Plasmonics for improved photovoltaic devices. *Nature Materials*. 2010;9: 205–213. https://doi.org/10.1038/nmat2629

9. Polat D. B., Eryilmaz L., Keles O. Generation of AgSi film by magnetron sputtering for use as anodes in lithium ion batteries. *ECS Meeting Abstracts*. 2015;MA2015-01: 514–514. https://doi.org/10.1149/ma2015-01/2/514

10. Liu B., Xu G., Jin C., ... Zhou L. The Si/Ag_2Si/Ag particles with the enhanced mechanical contact as anode material for lithium ion batteries. *Materials Letters*. 2020;280: 128536. https://doi.org/10.1016/j.matlet.2020.128536

11. Li R., Yang H., Zhang Y., ... Huang P. Physical mechanisms and enhancement of endurance degradation of SiO_x:Ag-based volatile memristors. *2023 Silicon Nanoelectronics Workshop (SNW)*. 2023;40: 117–118. https://doi.org/10.23919/SNW57900.2023.10183918

12. Ding X., Huang P., Zhao Y., Feng Y., Liu L. Understanding of the volatile and nonvolatile switching in Ag-based memristors. *IEEE Transactions on Electron Devices*. 2022;69: 1034–1040. https://doi.org/10.1109/TED.2022.3144373

13. Dias C., Lv H., Picos R., ...Ventura J. Bipolar resistive switching in Si/Ag nanostructures. *Applied Surface Science*. 2017;424: 122–126. https://doi.org/10.1016/j.apsusc.2017.01.140

14. Sarkar D. K., Cloutier F., El Khakani M. A. Electrical switching in sol-gel derived Ag-SiO_2 nanocomposite thin films. *Journal of Applied Physics*. 2005;97: 2–7. https://doi.org/10.1063/1.1870112

15. Jo S. H., Kim K. H., Chang T., Gaba S., Lu W. Si memristive devices applied to memory and neuromorphic circuits. In: *Proceedings of 2010 IEEE International Symposium on Circuits and Systems*, May 2010, IEEE; 2010. p. 13–16. https://doi.org/10.1109/iscas.2010.5537135

16. Huang C. Size-dependent behavior and challenges in Ag/Al_2O_3/Au memristors: an investigation into miniaturization effect. *Mechanical Engineering and Materials Science Independent Study*. 2023. https://doi.org/10.7936/r37p-cf73

17. Xu W., Wang J., Yan X. Advances in memristor-based neural networks. *Frontiers in Nanotechnology*. 2021;3: 645995. https://doi.org/10.3389/fnano.2021.645995

18. Zhang B., Kutalek P., Knotek P., ... Wagner T. Investigation of the resistive switching in Ag_xAsS_2 layer by conductive AFM. *Applied Surface Science*. 2016;382: 336–340. https://doi.org/10.1016/j.apsusc.2016.04.152

19. Jeong W. H., Han J. H., Choi B. J. Effect of Ag concentration dispersed in HfO_x thin films on threshold switching. *Nanoscale Research Letters*. 2020;15(1): 27 https://doi.org/10.1186/s11671-020-3258-6

20. Yoo J., Woo J., Song J., Hwang H. Threshold switching behavior of Ag-Si based selector device and hydrogen doping effect on its characteristics. *AIP Advances*. 2015;5(12): 127221. https://doi.org/10.1063/1.4938548

21. Ilyas N., Wang J., Li C., ... Li W. Controllable resistive switching of STO: Ag/SiO_2-based memristor synapse for neuromorphic computing. *Journal of Materials Science & Technology*. 2022;97: 254–263. https://doi.org/10.1016/j.jmst.2021.04.071

22. Cha J. H., Yang S. Y., Oh J., ... Choi S. Y. Conductive-bridging random-access memories for emerging neuromorphic computing. *Nanoscale*. 2020;12: 14339–14368. https://doi.org/10.1039/d0nr01671c

23. Sokolov A. S., Abbas H., Abbas Y., Choi C. Towards engineering in memristors for emerging memory and neuromorphic computing: a review. *Journal of Semiconductors*. 2021;42(1): 013101. https://doi.org/10.1088/1674-4926/42/1/013101

24. Raeis-Hosseini N., Lim S., Hwang H., Rho J. Reliable $Ge_2Sb_2Te_5$-integrated high-density nanoscale conductive bridge random access memory using facile nitrogen-doping strategy. *Advanced Electronic Materials*. 2018;4(11). https://doi.org/10.1002/aelm.201800360

25. Olesinski R. W., Gokhale A. B., Abbaschian G. J. The Ag-Si (Silver-Silicon) system. *Bulletin of Alloy Phase Diagrams*. 1989;10(6): 635–640. https://doi.org/10.1007/BF02877631

26. Anantharaman T. R., Luo H. L., Element W. Formation of new intermetallic phases in binary eutectic systems by drastic undercooling of the melt. *Nature*. 1966;210.(5040): 1040–1041. https://doi.org/10.1038/2101040a0

27. Terekhov V. A., Domashevskaya E. P., Kurganskii S. I., ... Agapov B. L. Formation of the Al_3Si metastable phase in Al-Si films obtained by ion-beam sputtering according to experimental and theoretical data. *Thin Solid Films*. 2023;772: 139816. https://doi.org/10.1016/j.tsf.2023.139816

28. Suryanarayana C. A new metastable phase in the silver-silicon system. *Journal of the Less Common Metals*. 1974;35(2): 347–352. https://doi.org/10.1016/0022-5088(74)90248-3

29. Lee W. S., Chen T. H., Lin C. F., Wu C. L. Microstructural evolution of nanoindented Ag/Si thin-film under different annealing temperatures. *Materials Transactions*. 2011;52(10): 1868–1875. https://doi.org/10.2320/matertrans.M2011160

30. Liu B., Xu G., Jin C., ... Zhou L. The Si/Ag_2Si/Ag particles with the enhanced mechanical contact as anode material for lithium ion batteries. *Materials Letters*. 2020;280: 128536. https://doi.org/10.1016/j.matlet.2020.128536

31. Materials Explorer Database. *Data retrieved from the Materials explorer for $AgSi_3$ (mp-978524) database: version 2025.06.09*. Available at: https://next-gen.materialsproject.org/materials/mp-978524

32. Materials Explorer Database. *Data retrieved from the Materials Explorer for Ag_3Si (mp-1219243) database: version 2025.06.09*. Available at: https://next-gen.materialsproject.org/materials/mp-1219243?material_ids=mp-1219243

33. Nakayama K. S., Nishijima M., Zhang Y., ... Suganuma K. Metastable phases of Ag–Si: amorphous Si and Ag-nodule mediated bonding. *Scientific Reports*. 2024;14(1): 1–9. https://doi.org/10.1038/s41598-024-70298-6

34. Cassidy C., Singh V., Grammatikopoulos P., ... Sowwan M. Inoculation of silicon nanoparticles with silver atoms. *Scientific Reports*. 2013;3: 1–7 https://doi.org/10.1038/srep03083

35. Barkov K. A., Terekhov V. A., Nesterov D. N., ... Sitnikov A. V. Formation of silver nanocrystals in Ag-Si composite films obtained by ion beam sputtering. *Condensed Matter and Interphases*. 2024;26(3), 407–416. https://doi.org/10.17308/kcmf.2024.26/12215

36. Zimkina T. M., Fomichev V. A. *Ultrasoft X-ray spectroscopy.*. Leningrad University Pub. House; 1971. 125 p.

37. Zimmermann P., Peredkov S., Abdala P. M., ... van Bokhoven J. A. Modern X-ray spectroscopy: XAS and XES in the laboratory. *Coordination Chemistry Reviews*. 2020;423: 213466. https://doi.org/10.1016/j.ccr.2020.213466

38. Terekhov V. A., Kashkarov V. M., Manukovskii E. Yu., Schukarev A. V., Domashevskaya E. P. Determination of the phase composition of surface layers of porous silicon by ultrasoft X-ray spectroscopy and X-ray photoelectron spectroscopy techniques. *Journal of Electron Spectroscopy and Related Phenomena*. 2001;114–116: 895–900. https://doi.org/10.1016/S0368-2048(00)00393-5

39. Blaha P., Schwarz K., Tran F., ... Marks L. D. WIEN2k: An APW+lo program for calculating the properties of solids. *The Journal of Chemical Physics*. 2020;152(7): 074101. https://doi.org/10.1063/1.5143061

40. Momma K., Izumi F. VESTA 3 for three-dimensional visualization of crystal, volumetric and morphology data. *Applied Crystallography*. 2011;44(6): 1272–1276. https://doi.org/10.1107/S0021889811038970

41. *SpringerMaterials: The Landolt-Börnstein Database. Data retrieved from the SpringerMaterials for Structural data № 0450926 database: version 2025*. Available at: https://materials.springer.com/isp/crystallographic/docs/sd_0450926

42. Langford J. I., Wilson A. J. C. Scherrer after sixty years: a survey and some new results in the determination of crystallite size. *Journal of Applied Crystallography*. 1978;11: 102–113. https://doi.org/10.1107/S0021889878012844

43. Hassanzadeh-Tabrizi S. A. Precise calculation of crystallite size of nanomaterials: a review. *Journal of Alloys and Compounds*. 2023:968: 171914. https://doi.org/10.1016/j.jallcom.2023.171914

44. Kurganskii S. I., Pereslavtseva N. S. Electronic structure of $FeSi_2$. *Physics of the Solid State*. 2002;44(4): 704–708. https://doi.org/10.1134/1.1470562

45. Kurganskii S. I., Pereslavtseva N. S. Electronic structure of cobalt disilicide film. *Physics of the Solid State*. 2000;42(8): 1542–1547. https://doi.org/10.1134/1.1307068

46. Pereslavtseva N. S, Kurganskii S. I. Electronic structure and spectral properties of nickel disilicide films. *Physics of the Solid State*. 1999;41(11): 1906–1910. https://doi.org/10.1134/1.1131124

47. Sarkar D. K., Dhara S., Nair K. G. M., Chowdhury S. Studies of phase formation and chemical states of the ion beam mixed Ag/Si (1 1 1) system. *Nuclear Instruments and Methods in Physics Research Section B: Beam Interactions with Materials and Atoms*. 2000;168(2): 215–220. https://doi.org/10.1016/S0168-583X(99)00876-9

48. Weijs P. J. W., Van Leuken H., De Groot R. A., ... Buschow K. H. J. X-ray-emission studies of chemical bonding in transition-metal silicides. *Physical Review B*. 1991;44(15): 8195. https://doi.org/10.1103/PhysRevB.44.8195

* *Translated by author of the article*

Information about the authors

Konstantin A. Barkov, Cand. Sci. (Phys.-Math.), Head of the Laboratory, Department of Solid State Physics and Nanostructures, Voronezh State University (Voronezh, Russian Federation).
https://orcid.org/0000-0001-8290-1088
barkov@phys.vsu.ru

Vitaly V. Babakov, student, Department of Solid State Physics and Nanostructures, Voronezh State University (Voronezh, Russian Federation).
https://orcid.org/0009-0002-8282-2034
babakov_vv@phys.vsu.ru

Gennady P. Potudansky, Lead Data Analyst, RT Labs JSC (Voronezh, Russian Federation).
https://orcid.org/0000-0002-4186-5081
potudanskiy@phys.vsu.ru

Sergey A. Ivkov, Cand. Sci. (Phys.-Math.), Leading Electronics Engineer, Department of Solid State Physics and Nanostructures, Voronezh State University (Voronezh, Russian Federation).
https://orcid.org/0000-0003-1658-5579
ivkov@phys.vsu.ru

Yaroslav A. Peshkov, Cand. Sci. (Phys.-Math.), Research Associate, Department of Solid State Physics and Nanostructures, Voronezh State University (Voronezh, Russian Federation).
https://orcid.org/0000-0003-0939-0466
tangar77@mail.ru

Ivan V. Polshin, student, Department of Solid State Physics and Nanostructures, Voronezh State University (Voronezh, Russian Federation).
https://orcid.org/0009-0008-7639-6538
polshin@phys.vsu.ru

Evgenii S. Kersnovsky, student, Department of Solid State Physics and Nanostructures, Voronezh State University (Voronezh, Russian Federation).
https://orcid.org/0009-0006-8215-6077
kersnovsky@phys.vsu.ru

Selby Y. Khydyrova, postgraduate student, Department of Electronic Technologies in Mechanical Engineering, Bauman Moscow State Technical University (Moscow, Russian Federation).
https://orcid.org/0000-0002-5510-0899
hydyrova@bmstu.ru

Konstantin M. Moiseev, Assistant Professor, Department of Electronic Technologies in Mechanical Engineering, Bauman Moscow State Technical University (Moscow, Russian Federation).
https://orcid.org/0000-0002-8753-7737
mkm430@ya.ru

Igor E. Zanin, Cand. Sci. (Phys.-Math.), Assistant Professor, General Physics Department, Voronezh State University (Voronezh, Russian Federation).
iezan@mail.ru

Alexandra K. Pelagina, Engineer-Physicist, Voronezh State University (Voronezh, Russian Federation).
Pisliaruk@phys.vsu.ru

Nikita S. Buylov, Cand. Sci. (Phys.-Math.), Assistant Professor, Department of Solid State Physics and Nanostructures, Voronezh State University; Engineer, Research Institute of Electronic Technology (Voronezh, Russian Federation).

https://orcid.org/0000-0003-1793-4400

buylov@phys.vsu.ru

Tran Van Tu, PhD, Lecturer, Faculty of Fundamental Sciences, Department of Physics, University of Medicine and Pharmacy at Ho Chi Minh city (Ho Chi Minh city, Viet Nam).

tranvantu@ump.edu.vn

https://orcid.org/0000-0002-3892-3578

Alexandr E. Nikonov, Cand. Sci. (Phys.-Math.), Research Engineer, Department of Solid-State Electronics, Voronezh State Technical University (Voronezh, Russian Federation).

nikonov.sasha1994@gmail.com

Aleksandr V. Sitnikov, Dr. Sci. (Phys.-Math.), Full Professor, Departments of Solid-State Electronics, Voronezh State Technical University (Voronezh, Russian Federation).

https://orcid.org/0000-0002-9438-9234

sitnikov04@mail.ru

Received January 29, 2025; approved after reviewing February 21, 2025; accepted for publication March 17, 2025; published online April 01, 2026.